

**SYNTHESIS OF ZnO AND STYRENE-ACRYLONITRILE-BASED
ELECTROLYTE FOR THE APPLICATION OF QUASI-SOLID-STATE
DYE-SENSITIZED SOLAR CELL**

by

TAN WEE CHING

**Thesis submitted in fulfillment of the requirements
for the degree of
Master of Science**

May 2011

ACKNOWLEDGEMENTS

I would like to express my deepest gratitude to my supervisors, Assoc. Prof. Dr. Ahmad Azmin Mohamad, and Mr. Ahmad Badri Ismail for their valuable contributions to this work, continuous support, enthusiasm, and patience. Their guidance is well-appreciated and I deeply believe that one could not possibly reach this far without such respectable supervision.

I would like to take this opportunity to express my gratitude to the university for the financial support through the Fellowship and Research University Postgraduate Research Grant Scheme. Likewise, I would also like to extend my gratitude to the School of Materials and Mineral Resources Engineering, Universiti Sains Malaysia for accommodating me during the conduct of my studies and for allowing me to use their facilities and equipment; the technical staff, Mr. Suhaimi Sulong and Mdm. Fong Lee Lee; and the administration staff, Mdm. Noor Hakishah Samsudin who also assisted me tremendously.

Thank you Mohd Najmi Masri, Muhammad Firdaus Mohd Nazeri, Mohd Hazwan Hussin, Aliyah Jamaludin, Siti Salwa Alias, and Jeremy Koh Chee Hao who have been giving me pieces of advice and encouragement unconditionally. Finally, I would like to thank my beloved family for the prayers, support, and inspiration amidst the challenges.

TAN WEE CHING

May 2011

LIST OF CONTENTS

	Pages
PROJECT TITLE	...i
ACKNOWLEDGEMENT	...ii
LIST OF CONTENTS	...iii
LIST OF FIGURES	...vii
LIST OF TABLES	...xiii
LIST OF ABBREVIATIONS	...xiv
LIST OF SYMBOLS	...xvi
ABSTRAK	...xviii
ABSTRACT	...xix
CHAPTER 1 INTRODUCTION	
1.0 Introduction	...1
1.1 Problem Statement	...3
1.2 Objectives	...5
1.3 Scope of Work	...5
CHAPTER 2 LITERATURE REVIEW	
2.0 Introduction	...6
2.1 Formation of Zinc Oxide via Zinc-Air System	...6
2.1.1 The Potential of Zinc-Air System as a New Zinc Oxide Synthesis Method	...11
2.1.2 Enhancement to the Formation of Zinc Oxide via Zinc-Air System	...13
2.1.3 Synthesis Profile of Zinc Oxide	...14

2.1.4 Characterizations of Zinc Oxide	...15
2.1.5 Formation Mechanism of Zinc Oxide	...18
2.1.6 Applicability of Zinc Oxide into Quasi-Solid-State Dye-Sensitized Solar Cell	...23
2.1.6.1 Zinc Oxide and Photosensitizers	...23
2.2 Iodide / Triiodide Redox Couple Gel Polymer Electrolyte	...25
2.2.1 Styrene-Acrylonitrile as Polymeric Host for Liquid Redox Electrolyte	...29
2.2.2 Characterizations for Gel Polymer Electrolyte	...33
2.3 Quasi-Solid-State Dye-Sensitized Solar Cell	...42
2.3.1 Components of Quasi-Solid-State Dye-Sensitized Solar Cell	...45
2.3.2 Quantitative Studies of a Quasi-Solid-State Dye-Sensitized Solar Cell	...46
 CHAPTER 3 EXPERIMENTAL	
3.0 Introduction	...49
3.1 Material and Experiment Apparatus	...49
3.1.1 Formation of Zinc Oxide via Zinc-Air System	...49
3.1.2 Preparation of Styrene-Acrylonitrile-based Redox Electrolyte	...50
3.1.3 The Assembly of Quasi-Solid-State Dye-Sensitized Solar Cell	...51
3.2 Synthesis of Zinc Oxide via Zinc-Air System	...51
3.3 Redox Electrolyte Preparation	...56
3.4 Quasi-Solid-State Dye-Sensitized Solar Cell Assembly	...61

CHAPTER 4 RESULTS AND DISCUSSION

4.0 Introduction	...64
4.1 Synthesis of Zinc Oxide via Zinc-Air System	...65
4.1.1 Synthesis Profiles of the Zinc-Air System	...65
4.1.2 Characteristic of Zinc Oxide Formed via Zinc-Air System	...70
4.1.2.1 Identification and Crystallinity Level via X-Ray Diffraction Test	...70
4.1.2.2 Morphological and Distribution Effect via Field Emission Scanning Electron Microscopy Observation	...77
4.1.2.3 Optical Property of Zinc Oxide Synthesized via the Zinc-Air System	...82
4.1.2.4 Structural Confirmation of Zinc Oxide via Transmission Electron Microscopy Observation	...87
4.1.3 The Effect of Elevated Drainage Currents at Room Temperature	...88
4.1.4 The Effect of Constant Drainage Current under Elevated Temperatures	...94
4.1.5 The Possible Growth Mechanism of Zinc Oxide in the Zinc-Air System	...96
4.2 Styrene-Acrylonitrile Based Electrolyte	...98
4.2.1 Bulk Resistance of Styrene-Acrylonitrile Based Electrolyte	...99
4.2.2 Mechanical Stability Evaluation via Shear Stress Vs Strain Rate Plot	...103
4.2.3 Conductivity, Viscosity and Diffusion Coefficient Property of Styrene-Acrylonitrile Based Electrolyte	...105

4.2.4 Bonds Identification Studies of Elevated Styrene-Acrylonitrile Composition via Fourier Transform Infra Red Spectroscopy	...108
4.2.5 Thermal-Conductivity Property of Styrene-Acrylonitrile Based Electrolyte	...111
4.2.6 Sodium Iodide / Iodine Liquid Electrolyte Encapsulated by Styrene-Acrylonitrile	...115
4.2.7 Stability of 19 wt.% Styrene-Acrylonitrile-Based Electrolyte for Quasi-Solid-State Dye-Sensitized Solar Cell Application	...118
4.3 Photocurrent-Photovoltage Characteristic of Assembled Quasi-Solid-State Dye-Sensitized Solar Cell	...119
CHAPTER 5 CONCLUSION AND RECOMMENDATIONS	
5.0 Conclusion	...122
5.1 Recommendation	...124
REFERENCES	...126
APPENDICES	
LIST OF PUBLICATION	

LIST OF FIGURES

Figure 2.1:	The schematic diagram of the O ₂ from ambient air permeabilize into the air-cathode in Zn-air batteries (Eom <i>et al.</i> , 2006).	...7
Figure 2.2:	The macrograph of Zn plate (a) before and (b) after synthesis at 50 mA cm ⁻² (Mohamad, 2006).	...9
Figure 2.3:	XRD results show ZnO formation as cause of failure in Zn-air system in hydroponics gel immersed in 6 M KOH (Mohamad, 2006).	...9
Figure 2.4:	The FESEM observation of formed ZnO detached from the anode of Zn-air system (a) front view and (b) cross section (Mohamad, 2006).	...10
Figure 2.5:	Schematic reaction of ZnO formation at the anodic Zn plate in hydroponic gel electrolyte (Mohamad, 2006).	...10
Figure 2.6:	Synthesis profiles of various battery systems (Linden and Reddy, 2002).	...15
Figure 2.7:	The crystal structure of wurtzite ZnO cell whereby two alternating planes of O ²⁻ and Zn ²⁺ are outlined for clarity (Modified from Coleman <i>et al.</i> , 2006 and Wang, 2004).	...16
Figure 2.8:	SEM shows highly densed nanorod arrays (Yuan <i>et al.</i> , 2010).	...17
Figure 2.9:	A compilation of (a) SEM image; (b) XRD identification; (c) growth structure; and (d) photoluminescence property of fabricated ZnO nanorods (Lee <i>et al.</i> , 2008).	...18
Figure 2.10:	SEM image of ZnO nanorods (Breedon <i>et al.</i> , 2009).	...19
Figure 2.11:	An example of a study on the effect of electrodeposition potential in 0.05 M Zn(NO ₃) ₂ aqueous solution (Xu <i>et al.</i> , 2009).	...20

Figure 2.12:	Effect of temperature of ZnO grown on Si (100) substrate: (a) 1200°C; (b) 1150°C; and (c) 1100°C (Al-Azri <i>et al.</i> , 2010).	...22
Figure 2.13:	A schematic diagram of N719 anchored to ZnO photoelectrode (Modified from Lee <i>et al.</i> , 2010).	...24
Figure 2.14:	SAN, a copolymer chain of styrene and acrylonitrile (Sigma Aldrich).	...29
Figure 2.15:	A schematic diagram of CTC formed and continuous I^- / I_3^- redox reaction (Modified from Ramani <i>et al.</i> , 1998).	...31
Figure 2.16:	A brief mechanism of chemically cross-linked gel electrolytes proposed by Murai <i>et al.</i> (2002).	...31
Figure 2.17:	Chemically crosslinking of poly(vinylpyridine-co-acrylonitrile) and Acros (Li <i>et al.</i> , 2007b).	...32
Figure 2.18:	Conductivity readings shows highest conductivity at 2.37 mS cm ⁻¹ with a varied concentration of NaI (10 mol% I ₂) (Lan <i>et al.</i> , 2006).	...32
Figure 2.19:	Series of conductivity values for different materials (Carraher, 2008).	...34
Figure 2.20:	Ionic conductivity of polyacrylonitrile-based electrolyte at 30°C for QSSC application (Wang <i>et al.</i> , 2004).	...35
Figure 2.21:	Diffusion Resistance, R_D value of the electrolyte (red line) of assembled Platinum / Polymeric Solid Electrolyte / Titanium Dioxide DSSC (Asano <i>et al.</i> , 2004).	...35
Figure 2.22:	An example of FTIR studies on pure (a) P(VdF-HFP) and P(VdF-HFP)-(PC / DEC / ACN)-LiI-I ₂ -TBP with the effect of different polymer contents; (b) 4 wt.%; (c) 6 wt.%; (d) 8 wt.%; and (e) 10 wt.% (Saikia <i>et al.</i> , 2008).	...37
Figure 2.23:	Temperature dependence conductivity of SAN based GPE (Lan <i>et al.</i> , 2006).	...38

Figure 2.24:	Temperature dependence conductivity of (a) polyethylene oxide consisting 0.5 M potassium iodide, 0.05 M I ₂ with different polymer content by Sharma <i>et al.</i> (2009).	...40
Figure 2.26:	An example of LSV measurement of poly(methyl methacrylate-co-styrene) (Jo <i>et al.</i> , 2003).	...41
Figure 2.26:	Schematic structure of dye-sensitized solar cell (Hara and Arakawa, 2002).	...44
Figure 2.27:	A schematic diagram of ZnTe, polymer electrolyte and ITO counter electrode assembled DSSC (Mohamad <i>et al.</i> , 2007).	...45
Figure 2.28:	An example of I-V curve of dark and illuminated Titanium Dioxide / N3 dye / Methoxypropionitrile / Lithium Iodide / Iodine DSSC (Regan <i>et al.</i> , 2002).	...47
Figure 2.29:	Photocurrent-voltage example of liquid electrolyte and gel electrolyte in a quasi-solid-state solar cell (Li <i>et al.</i> , 2007a).	...48
Figure 3.1:	The assembly of Zn-air system for ZnO synthesis (a) central body; (b) cylindrical caps; (c) attachment of the caps to the central body; and (d) the attachment of Zn foil onto the anode cap.	...52
Figure 3.2:	Process flow of the synthesis of ZnO photoanode via Zn-air system.	...55
Figure 3.3:	A schematic diagram on the assembly of PTFE casing for conductivity measurements.	...58
Figure 3.4:	Process flow of the preparation of SAN-based GPE for QSSC.	...60
Figure 3.5:	A schematic diagram of assembled ITO / SAN + NaI + I ₂ / N719 + ZnO + Zn QSSC.	...61
Figure 3.6:	Process flow of the ZnO and redox electrolyte assembly to form QSSC.	...63

Figure 4.1:	The combinations profile of synthesis current 10-80 mA at 27°C with inset of synthesis profile at 40, 50, 60, 70, and 80 mA.	...66
Figure 4.2:	The combinations profile of the effect of temperatures (27 to 90°C) at constant synthesis current, 10 mA.	...68
Figure 4.3:	XRD identification and effect of synthesis current on the crystallinity at 27°C.	...72
Figure 4.4:	The effect of synthesis current on the measured ZnO crystallite size.	...73
Figure 4.5:	XRD identification and effect of temperatures on crystallinity using a constant synthesis current of 10 mA.	...75
Figure 4.6:	The effect of synthesis temperature on the measured ZnO crystallite size.	...76
Figure 4.7:	FESEM observation of (a) a blank Zn foil before synthesis; and ZnO synthesized under various synthesis currents of (b) 10 mA; (c) 20 mA; (d) 30 mA; (e) 40 mA; (f) 50 mA; (g) 60 mA; (h) 70 mA; and (i) 80 mA at room temperature.	...79
Figure 4.8:	FESEM observation of (a) a blank Zn foil before synthesis; and ZnO synthesized at 10 mA under various temperatures of (b) 27°C; (c) 30°C; (d) 40°C; (e) 50°C; (f) 60°C; (g) 70°C; (h) 80°C; and (i) 90°C.	...81
Figure 4.9:	Low count of the UV-Vis Spectroscopy results by ZnO synthesized via the Zn-air system.	...82
Figure 4.10:	Photoluminescence spectra of ZnO synthesized via the Zn-air system with the effect of synthesis current.	...83
Figure 4.11:	Photoluminescence spectra of ZnO synthesized via the Zn-air system with the effect of temperature.	...86

Figure 4.12:	Needle-like structure with a pointed end diameter of ~ 20 nm from an optimized sample formed by synthesizing at 10 mA under 27°C.	...88
Figure 4.13:	Effect of synthesis currents on the lattice parameter.	...89
Figure 4.14:	Proposed lattice mismatch of formed ZnO with its Zn substrate.	...90
Figure 4.15:	Schematic diagram on the suggested formation of the ZnO rosette-like structure (a) normal formation along the Z-axis; (b) downwards enlargement of needle-like ZnO; and (c) diverted formation along the (101) plane.	...93
Figure 4.16:	Effect of synthesis temperature on the lattice parameter.	...94
Figure 4.17:	Proposed formation mechanism of ZnO: (a) predominant ZnO; (b) initiator ZnO centers form above a predominantly ZnO layer; (c) continuous growth of ZnO; (d) linked 'valley' of needle-like structure due to the continuous release of Zn(OH)_4^{2-} ; and (e) ZnO and zinc separation with very saturated Zn(OH)_4^{2-} content.	...97
Figure 4.18:	Nyquist plots of elevated content of SAN in NaI / I ₂ based electrolyte.	...100
Figure 4.19:	Logarithmic imaginary impedance with the function of frequency as to determine the α value range as the increase of SAN content.	...103
Figure 4.20:	A comparison of τ vs γ plots with the effect of elevated SAN content.	...104
Figure 4.21:	The value range of conductivity and viscosity between 0-24 wt.% SAN content and its optimized 19 wt.% SAN.	...106
Figure 4.22:	The value of D increases and then decreases which reflects a sudden attractive force of both I^- and I_3^- towards phenyl group upon addition of SAN.	...107

Figure 4.23:	FTIR indicated only an elevated peak at 706 cm^{-1} with higher concentration of SAN in liquid electrolyte mixture.	...109
Figure 4.24:	The effect of SAN content to the value of R_b with temperature.	...112
Figure 4.25:	A comparison of thermal dependence plot of liquid electrolyte and SAN-based electrolyte ranging from 4 to 24 wt.% under elevated temperatures.	...113
Figure 4.26:	A schematic diagram of SAN coils in (a) $< 19\text{ wt.}\%$; (b) $19\text{wt.}\%$; and (c) $> 19\text{ wt.}\%$ SAN.	...115
Figure 4.27:	Redox activities in SAN were proposed in the magnified structure that consists of $19\text{ wt.}\%$ SAN.	...116
Figure 4.28:	LSV indications of $19\text{ wt.}\%$ SAN-based electrolyte shows the stability window between -1.68V and 1.38V118
Figure 4.29:	Photocurrent-photovoltage characteristic of assembled QSSC.	...120

LIST OF TABLES

Table 2.1:	Properties of Zn-air system in comparison with other systems of the same range (Linden and Reddy, 2002). Note: 1 to 8-best to poorest.	...13
Table 3.1:	The composition of redox electrolyte with SAN as polymer host.	...57
Table 4.1:	An approximate calculation of distance of Zn^{2+} arrays in along (100) plane based on the value of a . 6 th position of Zn and 5 th position of ZnO showed a rather similar position, distanced from the left in Figure 4.14.	...90
Table 4.2:	Band assignment of 'standard' liquid electrolyte without and with SAN.	...110

LIST OF ABBREVIATIONS

CTC	Charge Transfer Complex
ATR	Attenuated Total Reflectance
CPE	Constant Phase Element
DLE	Deep Level Emission
DSSC	Dye-Sensitized Solar Cell
dye ⁺	Excited Dye
e ⁻	Free Electron
EC	Ethylene Carbonate
E _g	Band Gap Energy
FESEM	Field Emission Scanning Electron Microscopy
FRA	Frequency Response Analyzer
FTIR	Fourier Transform Infra Red Spectroscopy
FWHM	Full Width at Half Maximum
GPE	Gel Polymer Electrolyte
ICDD	International Center of Diffraction Data
<i>I_{DLE}</i>	Photoluminescence Intensity of Deep Level Emission
ITO	Indium Tin Oxide
<i>I_{UV}</i>	Photoluminescence Intensity of Ultraviolet Emission
I-V	Photocurrent – Photovoltage
LSV	Linear Sweep Voltammetry

N719	Bis(tetrabutylammonium)-cis-(dithiocyanato)-N, N0-bis(4-carboxylate-40-carboxylic acid-, 20-bipyridine) ruthenium (II)
PC	Propylene Carbonate
PL Spec	Photoluminescence Spectroscopy
PTFE	Polytetrafluoroethylene
QSSC	Quasi-Solid-State Dye-Sensitized Solar Cell
SAN	Styrene-Acrylonitrile
SEM	Scanning Electron Microscopy
TEM	Transmission Electron Microscopy
UV-Vis	Ultraviolet-Visible Spectroscopy
XRD	X-Ray Diffraction
Zn-air	Zinc-Air

LIST OF SYMBOLS

T_{hkl}	Coefficient of Texture
$I_m(hkl)$	Measured Relative Intensity of the (hkl) Plane
$I_o(hkl)$	Standard Intensity of the Sample Data
n	Number of XRD Peaks
γ	Strain Rate
A	Intact Area of Electrolyte
C_o	Initial Concentration of Reducible Substance
C_{sh}	Shunt Conductivity
D	Diffusion coefficient
E_a	Activation Energy
F	Faraday's Constant
f	Frequency
I_c	Current
I_{sc}	Short Circuit Current
J_p	Photocurrent
k	Boltzmann constant
r	Radius of spherical
R_b	Bulk Resistance
R_f	Interfacial Resistance
R_s	Solution Resistance
T	Temperature
t	Time
t_e	Thickness of Electrolyte
V_{ext}	Measurement Voltage
V_i	Cell Internal Voltage

V_{oc}	Open Circuit Voltage
Z'	Real Impedance
Z''	Imaginary Impedance
η	Viscosity
η_e	Number of Electron
σ	Bulk conductivity
σ_0	Pre-exponential factor
τ	Shear Stress
ω	Phase Shift

**SINTESIS ZnO MELALUI SISTEM ZINK-UDARA DAN
PENGUNAAN ELEKTOLIT BERASASKAN STIRENA-AKRILONITRIL
UNTUK SEL SURIA BERPEKAAN PENCELUP DALAM KEADAAN
PEPEJAL SEPARA**

ABSTRAK

Sintesis zink oksida (ZnO) melalui sistem zink-udara (Zn-udara) telah dikaji. ZnO telah terbentuk apabila sistem Zn-udara dinyahcaskan sepenuhnya. Potensi pembangunan Zn-udara sebagai salah satu alternatif kepada kaedah sintesis ZnO telah dikaji untuk mencari nisbah luas kepada isipadu tertinggi berdasarkan beberapa kajian pencirian seperti pembelauan sinar-X, mikroskopi imbasan elektron pancaran medan, spektroskopi foto pendarkilau dan mikroskopi transmisi elektron. Kajian menunjukkan nisbah luas kepada isipadu dan pancaran ultralembayung tertinggi dihasilkan oleh sampel yang disintesis menggunakan arus 10 mA pada suhu bilik. Jejaram ZnO berhablur tinggi yang terbentuk berukuran ~ 20 nm pada hujung tajamnya manakala ~ 65 nm pada dasarnya. Kebolegunaan ZnO yang telah disintesis juga dikaji berdasarkan perhimpunan sel suria berpekaan pencilup dalam keadaan pepejal separa (QSSC). Oleh yang demikian, stirena-akrilonitril (SAN) diperkenalkan dalam sistem untuk menempatkan elektrolit redoks cecair dan memberi kestabilan mekanikal. Komponen elektrolit ini juga dikaji untuk menentukan keseimbangan nilai konduktiviti dan kelikatan. Elektrolit polimer gel dengan komposisi optimum 0.5 M natrium iodida + 0.05 M iodin + 19 wt.% SAN memberikan nilai konduktiviti 1.49 mS cm^{-1} dan kelikatan 1.4 Pa s. Akhirnya, plot fotoarus – fotovoltan oleh QSSC yang dihimpunkan menunjukkan respon positif terhadap kebolegunaan ZnO yang disintesis melalui sistem Zn-udara.

**SYNTHESIS OF ZnO VIA ZINC-AIR AND
APPLICATION OF STYRENE-ACRYLONITRILE-BASED ELECTROLYTE
FOR QUASI-SOLID-STATE DYE-SENSITIZED SOLAR CELL**

ABSTRACT

The synthesis of zinc oxide (ZnO) via the zinc-air (Zn-air) system was studied. The ZnO was formed upon discharge completion of the Zn-air system. Potential development of Zn-air as an alternative to ZnO synthesis method was studied to seek the highest surface-to-volume ratio based on the X-ray diffraction, field emission scanning electron microscopy, photoluminescence spectroscopy, and transmission electron microscopy characterization studies. Studies showed that the highest surface-to-volume ratio and ultraviolet emission sample can be fabricated at synthesis current as low as 10 mA at room temperature. Highly crystalline ZnO needle-like formed, measured at ~ 20 nm at the tip and ~ 65 nm at the base. The usability of the synthesized ZnO was also studied based on a quasi-solid-state dye-sensitized solar cell (QSSC) assembly. In order to do so, styrene-acrylonitrile (SAN) was introduced into encapsulating liquid redox electrolyte to give mechanical stability to the system. This SAN-based electrolyte component in QSSC was also studied to optimize its conductivity and viscosity properties with an optimum composition of 0.5 M sodium iodide + 0.05 M iodine + 19 wt.% SAN. The gel polymer electrolyte exhibits conductivity value of 1.49 mS cm⁻¹ and viscosity value of 1.4 Pa s. Finally, the photocurrent – photovoltage plot of assembled QSSC showed positive response of the usability of ZnO synthesized via Zn-air system.

CHAPTER 1

INTRODUCTION

1.0 Introduction

The zinc-air (Zn-air) system is conventionally known as a primary battery system. A Zn-air battery consists of a zinc (Zn) foil anode, an electrolyte, normally potassium hydroxide (KOH), and an air-cathode (Bender *et al.*, 2002). The air-cathode absorbs and reduces oxygen from the ambient air into hydroxyl [OH⁻] ions that react with released anodic Zn ions [Zn²⁺] to produce power supply. The Zn-air system is simple, convenient, inexpensive and lightweight, and is used as a power source for portable electronic devices.

However, the Zn-air battery fails upon discharge completion. Just like any other types of primary battery system, the Zn-air system cannot be recharged for multiple use. Tons of these used batteries remain useless in landfills which do not only cause serious health problems but also pollution problems (Espinosa *et al.*, 2004). Such problems should be curbed through recycling. The potential of Zn-air system to be recycled has yet to be explored in depth. It was first reported that the failure of the Zn-air system was due to the formation of zinc oxide (ZnO) at the Zn anode (Mohamad, 2006).

Meanwhile, ZnO is one of the most promising candidates in today's semiconducting industry. Thus, the practicality of Zn-air system can be proposed as a new synthesis method to form ZnO. The key aspect of the formation of ZnO during Zn-air discharge is its ability to draw ambient oxygen (O₂) from air to its cathode as the oxidizing agent (Eom *et al.*, 2006). The infinite use of the air-cathode adds an advantage on the reusability of the Zn-air system, once a fresh Zn anode is being replaced. Hence, Zn-air system could provide a win-win solution for waste reduction as well as a new ZnO synthesis method to meet its demands today.

Based on previous works, the formation of ZnO was confirmed via the X-ray diffraction (XRD) measurement and a rod-like structure was observed at the anode of the Zn-air system via field emission scanning electron microscopy (FESEM) (Masri and Mohamad, 2009). To date, the studies on the formation of ZnO via Zn-air system were very few using this method. The development, applicability, and potential of ZnO formed via Zn-air system needs to be explored to meet the rising demands for various semiconducting applications such as the dye-sensitized solar cell (DSSC).

ZnO is currently favored with its rising application in DSSC. During solar harvesting, ZnO is able to excite and inject electrons into its conduction band to be extracted to an external load or application and back to the counter electrode (Soga and Tetsuo, 2006). Redox couple of iodide / triiodide [I^- / I_3^-] in the liquid electrolyte completes the photon-to-current energy conversion cycle.

However, a few problems occur with the applications of liquid electrolytes such as leakage, solvent evaporation, high-temperature instability, photochemical degradation, and sealing issue (Mohamad *et al.*, 2007). This will further elevate the difficulties of liquid electrolyte placement between the electrodes of DSSC. Thus, embedding a polymer as host such as styrene-acrylonitrile (SAN) to provide mechanical stability to the liquid-based electrolyte could be done to curb the said matters.

SAN offers good chemical and heat resistance, high clarity plus better ultra-violet resistance compared to acrylic alone in the DSSC system. It also has the ability to contain redox liquid electrolyte for it possesses a phenyl group having certain affinity towards iodine, I_2 (Ramani *et al.*, 1998). This attraction force enables I_2 to seep through the polymeric network structure that encapsulates the I_2 thus providing mechanical stability to the electrolyte. Hence, the embedment of SAN into the DSSC forms a quasi-solid-state dye-sensitized solar cell (QSSC).

This basically leads to potential development of Zn-air system as a new alternative method in synthesizing the ZnO, as well as the applicability of SAN-based electrolyte in the QSSC system.

1.1 Problem Statement

The simplicity of ZnO formation creates a vast variety in its synthesis methods. However, these methods have certain procedure that needs much attention and attentive handling (Al-Hajry *et al.*, 2009), abundant supporting precursors (Chen *et al.*, 2006), high end equipment (Lu *et al.*, 2007), and some even a power supply

(Wu *et al.*, 2006c). Among the available methods, the potential of Zn-air system for synthesizing ZnO still remains unexplored. This system will not only provide solution for good battery disposal but also to recycle the waste product as a valuable source.

To date, research works on the formation of ZnO via Zn-air system remains stagnant. Further elaboration necessary to establish best synthesis handling in promoting the formation of ZnO via the Zn-air system has yet to be reported. The mechanism of failure and the formation of ZnO layer at this anode are still unknown. This aspect of study is crucial to control the possible parameters involved in the formation of ZnO via the Zn-air method.

The usability of ZnO synthesized via Zn-air system has remained questionable. In order to measure its usability, synthesized ZnO was sandwiched with a SAN-based gel polymer electrolyte (GPE) to form a QSSC. Lan *et al.* (2006) reported the application of SAN with various salt concentrations. However, the amount of SAN content necessary to encapsulate the liquid redox electrolyte has remained questionable. Polymeric compositional studies are essential in determining the balanced level between conductivity value and mechanical support. The conduction mechanism in SAN-based electrolyte has also remained unknown. It is also important to ensure continuous solar harvesting.

ZnO synthesized via Zn-air system and SAN-based electrolyte signify the characteristics of both photoanode and redox electrolyte of the QSSC. However, the workability of these two components is unknown and questionable.

1.2 Objectives

The main objectives of this study are as follows:

- i. To study the performance of the Zn-air system in forming the highest surface-to-volume ZnO ratio structure;
- ii. To measure the optimum conductivity and mechanical stability of SAN-based redox electrolyte; and
- iii. To assemble and characterize the QSSC based on prepared ZnO and SAN-based redox electrolyte.

1.3 Scope of Work

The scope of work governs:

- i. The study on ZnO formation via Zn-air system which includes the effect of:
 - discharge currents of 10, 20, 30, 40, 50, 60, 70, and 80 mA at constant room temperature and
 - temperatures of 27, 30, 40, 50, 60, 70, 80, and 90°C at constant 10 mA discharge current;
- ii. The preparation of polymeric-based electrolyte which includes the effect of SAN composition of 4, 8, 12, 16, 19, 20, and 24 wt% in constant redox solution of 0.5 M NaI and 0.05 M I₂; and
- iii. The assembly of the QSSC to study the workability of both (i) and (ii).

CHAPTER 2

LITERATURE REVIEW

2.0 Introduction

This chapter reviews on the project background, the fabrication of its components and, the development of this project. It also tackles the advantages of a few simple alternatives to today's fabrication and devices technology reviews, and literature of the fabrication of:

- i. Zinc oxide (ZnO) synthesized via zinc-air (Zn-air) system;
- ii. Styrene-acrylonitrile (SAN) based gel polymer electrolyte (GPE);
and
- iii. Quasi-solid-state dye-sensitized solar cell (QSSC).

The simplicity of using Zn-air system as an alternative to synthesize ZnO and the introduction of SAN for liquid electrolyte encapsulation for continuous solar harvesting and safety factor are also included.

2.1 Formation of Zinc Oxide via Zinc-Air System

The Zn-Air is a well known battery system with a special feature that only the active component of the negative electrode, zinc (Zn) needs to be stored in the system, while the reactant for the positive electrode, oxygen (O₂) is drawn from the air during discharge (Wang *et al.*, 2003). Potassium hydroxide (KOH) aqueous solution was used as the electrolyte while, atmospheric O₂ acts as a depolarizing agent in the electrochemical system diffusing into the cell and as an inconsumable cathodic reaction site with the cell's electrolyte (Bender *et al.*, 2002).

The abundance of O₂ from the environment surrounding the system has an advantage of being an infinitely inconsumable cathode. Figure 2.1 shows the schematic air flow of the cathode material as it catalytically promotes the reduction of O₂ in the presence of an aqueous alkaline electrolyte. Further studies of the O₂ flowing into the air-cathode pertain to the works of Eom *et al.* (2006). Theoretically, the air-cathode has an infinite useful life and physical size, and its electrochemical properties remain constant during discharge (Mohamad, 2006).

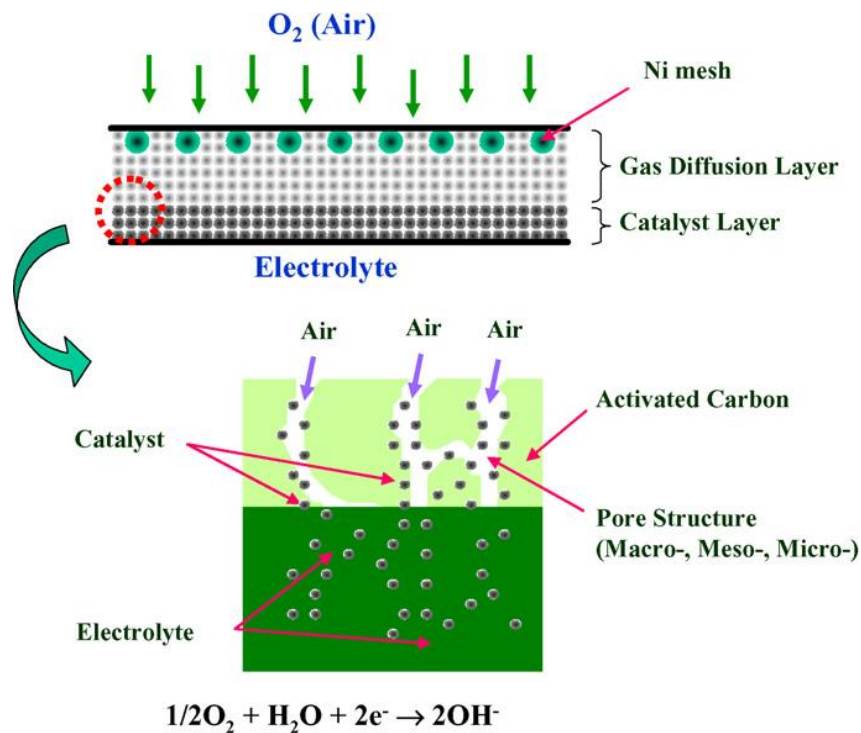


Figure 2.1: The schematic diagram of the O₂ from ambient air permeabilize into the air-cathode in Zn-air batteries (Eom *et al.*, 2006).

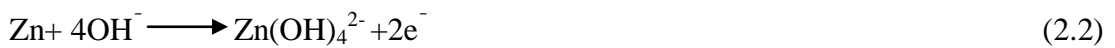
Since the air-cathode has infinite life, the electrical capacity of the system is determined only by the Zn anode capacity (Bender *et al.*, 2002). The low equilibrium potential and high over-potential for hydrogen reaction make Zn an element with the lowest standard potential among all elements that can be reduced from aqueous electrolytes in Zn-air system (Smedley and Zhang, 2007).

Hence, whenever a Zn-air is exposed to a limitless supply of ambient air, this system reduces the O₂ from air and water (H₂O) from the electrolyte to give hydroxyl ions [OH⁻] (Equation 2.1). These OH⁻ then reacts with Zn to give zincate ions [Zn(OH)₄²⁻] thereby enabling it to generate free electron by itself without any external force such as current supply (Equation 2.2). Free electron will then be needed back at the air-cathode to support O₂ reduction as a loop, as shown by Equation (2.1-2.4) (Mohamad, 2006; Deiss *et al.*, 2002):

At air-cathode:



At Zn anode:



Overall:



This reduction decreases the Zn-air battery performance when it degrades the Zn anode surface into a whitish oxide layer as shown in Figure 2.2. Deiss *et al.* (2002) proposed that ZnO was formed and remained on the Zn electrode after having been charged and even after the discharge over a total of three cycles. In later years, Mohamad (2006) proved that the cause of the Zn electrode degradation was identified to be ZnO via X-ray diffraction (XRD) as shown in Figure 2.3.

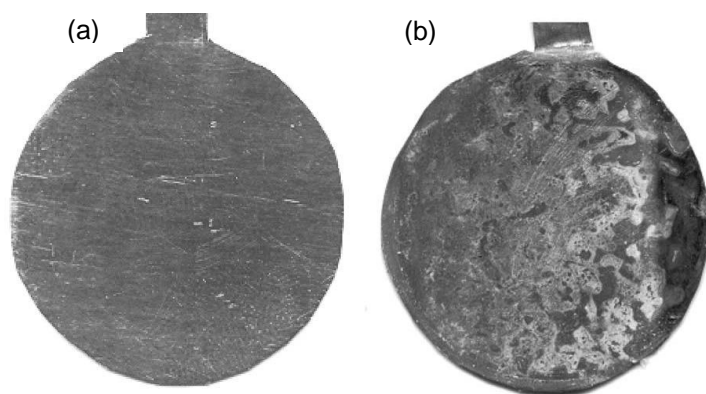


Figure 2.2: The macrograph of Zn plate (a) before and (b) after synthesis at 50 mA cm^{-2} (Mohamad, 2006).

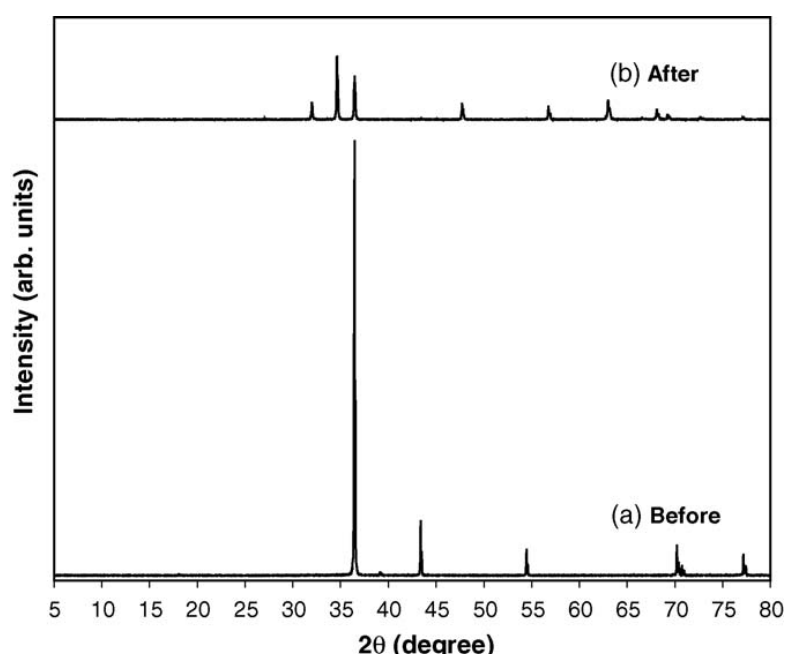


Figure 2.3: XRD results show ZnO formation as cause of failure in Zn-air system in hydroponics gel immersed in 6 M KOH (Mohamad, 2006).

Further observation under the field emission scanning electron microscopy (FESEM) for ZnO formed at 50 mA cm^{-2} are shown in Figure 2.4a-b. An overview on how the Zn-air system works is shown by a schematic diagram in Figure 2.5 with the formation of ZnO in a hydroponic gel-based KOH electrolyte (Mohamad, 2006).

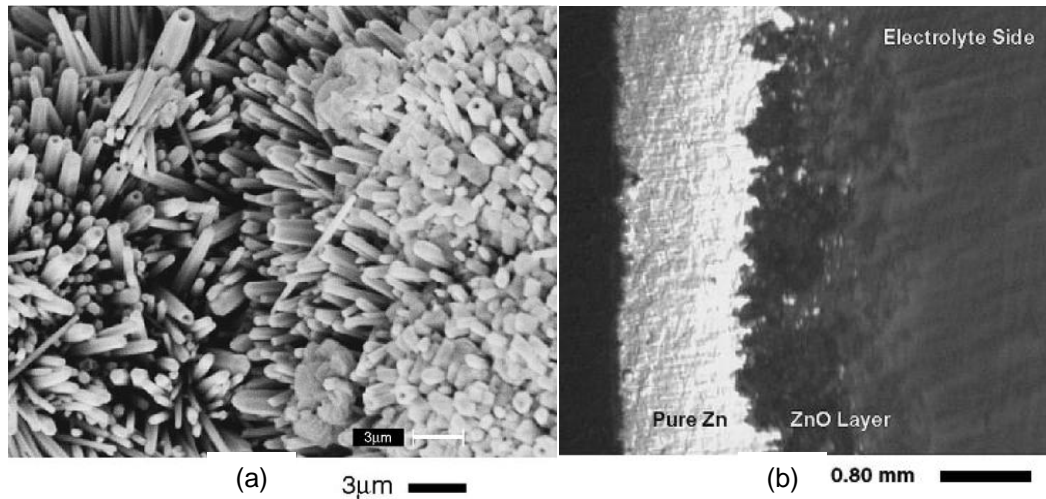


Figure 2.4: The FESEM observation of formed ZnO detached from the anode of Zn-air system (a) front view and (b) cross section (Mohamad, 2006).

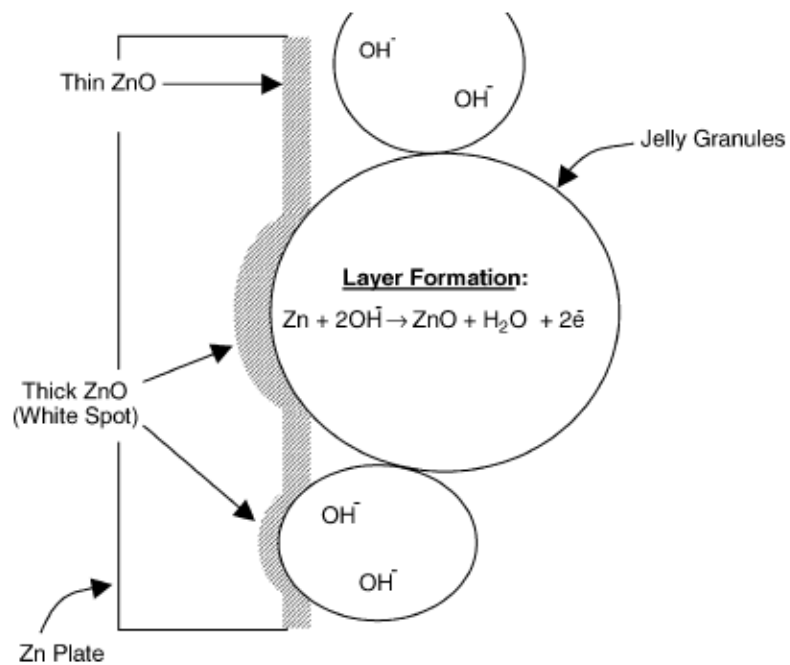


Figure 2.5: Schematic reaction of ZnO formation at the anodic Zn plate in hydroponic gel electrolyte (Mohamad, 2006).

Due to the fact that the formation of ZnO occurred in the Zn-air system, these primary batteries were not rechargeable. This weakness has led to a slow development of the Zn-air battery. However, the Zn-air system could be made reusable and can offer an exciting potential as a new ZnO synthesizing method.

2.1.1 The Potential of Zinc-Air System as a New Zinc Oxide Synthesis Method

The ZnO is unique whereby a variety of ZnO morphologies such as nanobelts (Wang, 2004), nanowires (Wang *et al.*, 2005b), nanorings (Wang, 2004), nanopellets (Chiu *et al.*, 2008), nanorods (Li *et al.*, 2009), nanotetrapods (Wang *et al.*, 2005a), and nanotubes (Zhou *et al.*, 2008) have been synthesized and touted to have applications in optoelectronics, sensors, transducers, and the biomedical science.

These aligned one-dimensional ZnO nanostructures have attracted much attention in recent years, particularly as electron accepting semiconductors in electro-photo-mechanical nanodevices and organic solar cells (Teki *et al.*, 2008). The ZnO is widely known due to its variation of nanostructures and synthesis flexibility (Boschloo *et al.*, 2006). Thus, much research on its fabrication techniques and process has been carried out to optimize the characteristics of ZnO.

Rapid heating (Wang *et al.*, 2005a), vapor phase transport (Yang *et al.*, 2008b), direct current magnetron sputtering (Teki *et al.*, 2008), thermal evaporation (Umar *et al.*, 2008), hydrothermal (Zhou *et al.*, 2008), solid-vapor sublimation (Wang, 2004), electrodeposition (Elias *et al.*, 2007), and pyrolysis (Chiu *et al.*, 2008) are the few types of ZnO fabrication methods. These methods have been reported to successfully form ZnO nanotetrapods (Wang *et al.*, 2005a), nanorods (Teki *et al.*, 2008), nanonails (Umar *et al.*, 2008), nanobelts, nanorings, nanosprings (Wang, 2004), and nanowires (Elias *et al.*, 2007).

The simplest method is the decomposition of ZnO, however it requires very high temperature (~ 1400 °C). Another direct method is to heat the Zn powder in an O₂ atmosphere wherein the required temperature is lower (~ 600 °C), but it needs careful monitoring of the vapor pressures of Zn and O₂ (Teki *et al.*, 2008). The anodization technique, for example, is one of the most versatile surface treatments to produce oxide films (Kim and Choi, 2008). However, this preparations method requires additional apparatus such as expensive reference electrode, deaeration or agitation system, and current supply in order to form ZnO.

In actual scenario, the overall cost in utilizing these few conventional synthesis methods may rise high enough to meet market demands. These varieties of ZnO fabrication methods involve many procedures and handling precautions in order to fabricate decent ZnO structures. Thus, by eliminating such hassles, it will indeed serve as an incentive to market demands. These hassles can be overcome in another compatible method, which is the Zn-air method.

The Zn-air system does not need high temperature, chelating agent, agitation, deaeration, coating, heat treatment, and power supply to form comparable ZnO structures. This system is able to save up a number of procedures, handling, and attention, amount and costs for extra reactants, cathode material, setup equipments, and input energy. Moreover, Zn-air technique differs from other ZnO synthesis techniques whereby the whole system could be reused again once ZnO formation is achieved.

The reconstruction was not needed wherein the air-cathode was reported to have infinite lifetime upon discharge (Mohamad, 2006). The electrolyte that intermediates anode and cathode consisting of KOH aqueous based solution can be reused even after ZnO is formed at the anode (Goldstein *et al.*, 1999). Even when the OH⁻ was consumed based on Equation 2.2 it was also returned (Equation 2.3), retaining an inconsumable electrolyte. Thus, the idea of Zn-air system can be implemented to create a recyclable or reusable alternative to current ZnO synthesis method.

2.1.2 Enhancement to the Formation of Zinc Oxide via Zinc-Air System

The formation of ZnO was due to the failure of the battery system. The formation of ZnO can be enhanced via ‘*promoting*’ failure of the weaknesses of Zn-air system as in battery mechanism. There are many factors that determine the synthesis rate of this system. Table 2.1 shows the tabulated comparison of Zn-air system with other battery systems of the same range.

Table 2.1: Properties of Zn-air system in comparison with other systems of the same range (Linden and Reddy, 2002). Note: 1 to 8 – best to poorest.

System	Voltage	Specific energy (gravimetric)	Power density	Flat discharge profile	Low-temperature operation	High-temperature operation	Shelf life	Cost
Zinc/carbon	5	4	4	4	5	6	8	1
Zinc/alkaline/manganese dioxide	5	3	2	3	4	4	7	2
Magnesium/manganese dioxide	3	3	2	2	4	3	4	3
Zinc/mercuric oxide	5	3	2	2	5	3	5	5
Cadmium/mercuric oxide	6	5	2	2	3	2	3	6
Zinc/silver oxide	4	3	2	2	4	3	6	6
Zinc/air	5	2	3	2	5	5	—	3
Lithium/soluble cathode	1	1	1	1	1	2	2	6
Lithium/solid cathode	1	1	2	2	2	3	2	4
Lithium/solid electrolyte	2	1	5	2	6	1	1	7

* 1 to 8—best to poorest.

Two factors for promoting ZnO formation were observed: (i) was not able to provide high potential synthesis capacity and (ii) Zn-air did not work well in high ambient temperature. Thus, there is a strong reason to believe that ZnO formation can be promoted based on the weaknesses of Zn-air, such as high capacity drainage rates and the need to discharge it at high ambient temperature under a very low cost (Linden and Reddy, 2002). Thus, the enhancement of ZnO synthesis can be conducted with the effect of (i) current and (ii) under different ambient temperatures.

2.1.3 Synthesis Profile of Zinc Oxide

The performance of batteries is determined by its discharge profile. The discharge curves show the stability of drained potential with its battery capacity. These discharge curves will not be used to observe and maintain the discharge stability, potential, and durability of the system but to observe its duration upon the completion of ZnO formation and to indicate the completion assurance of its formation saturation. A comparison of the discharge curves of the major primary batteries is shown in Figure 2.6 wherein most of the battery types have a relatively flat discharge profiles. Based on the highlighted line in Figure 2.6, it can be concluded that the saturation of ZnO formation on the surface of Zn anode starts to block further electrochemical reactions as shown by the zeroed curve.

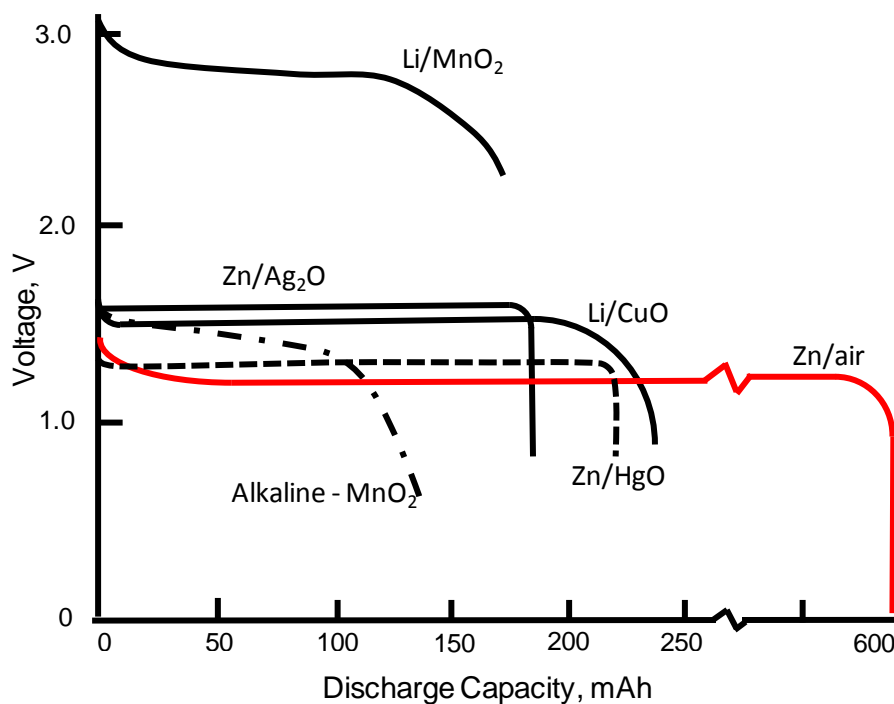


Figure 2.6: Synthesis profiles of various battery systems (Linden and Reddy, 2002).

As to synthesize ZnO via Zn-air system, this profile was used to document system stability to ensure continuous and constant Zn(OH)_4^{2-} supply and further known as the ZnO synthesis profile. Its synthesis duration will further enhance the description of ZnO formation under both elevated synthesis current and temperature conditions in the Zn-air system based on the next characterization levels. Note that these synthesis curves of Zn-air system do not primarily indicate good saturated ZnO formation and may only be determined under highly magnified observation.

2.1.4 Characterizations of Zinc Oxide

The ZnO, a II-VI compound, n-type semiconducting metal oxide in solar cell is normally hexagonal (wurtzite) structured as shown in Figure 2.7. The ZnO has a wide direct band gap of 3.37 eV suitable for short-wavelength optoelectronic devices such as ultra violet detectors and light emitting diodes (Guzman *et al.*, 2009).

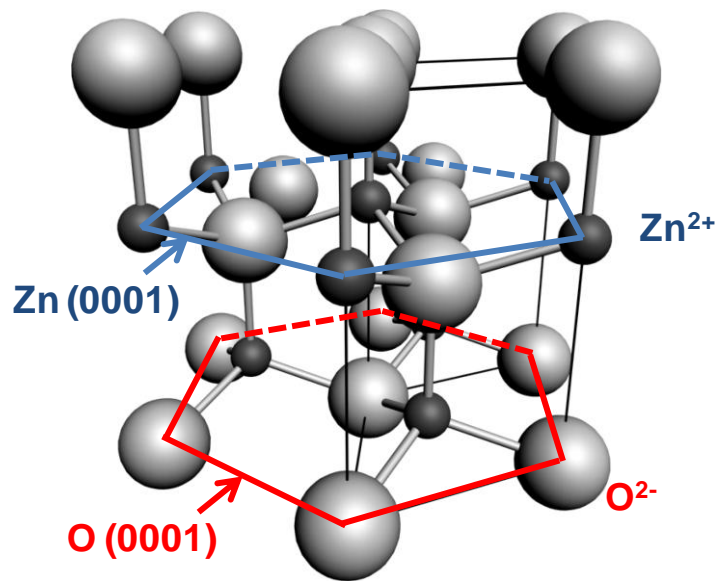


Figure 2.7: The crystal structure of wurtzite ZnO cell whereby two alternating planes of O^{2-} and Zn^{2+} are outlined for clarity (Modified from Coleman *et al.*, 2006 and Wang, 2004).

The large binding energy of 60 meV gives higher resistance for exciton recombination compatible for applications such as room temperature exciton laser in the ultraviolet range and as protective ultra violet-absorbing additive in skin cream to advanced rubber composites. The ZnO is a transparent oxide that exhibits semiconducting, piezoelectric, and pyroelectric multiple properties. Its conductivity is due to the non-stoichiometry consisting of excess metal which provides higher charge carrier mobility compared to other oxides, such as titanium dioxide (Boschloo *et al.*, 2006).

In materials engineering, miniaturization is currently the main objective of most ZnO-based device assembly. For example, the basic physical requirement for higher solar harvesting efficiency is generally effected by more photons being exposed to higher ZnO surface area in a smaller space allocated. To date, no study on this aspect has yet been made for the ZnO synthesized via Zn-air system. Thus, an

example of highly dense nanorod structure as shown by Scanning Electron Microscopy (SEM) image in Figure 2.8 is desired.

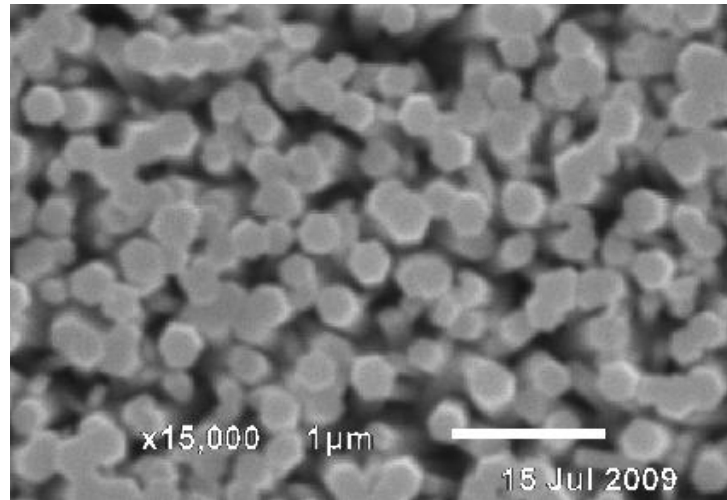


Figure 2.8: SEM shows highly dense nanorod arrays (Yuan *et al.*, 2010).

Other factors such as impurities, composition, and property can also be detected by characterization tests such as XRD and Photoluminescence Spectroscopy (PL Spec). These characterizations on ZnO synthesized via Zn-air system are yet to be explored. Thus, as an example, Figure 2.9 shows a work compilation by Lee *et al.* (2008). Based on SEM image in Figure 2.9a, it is observed that nanorods agree with the hexagonal wurtzite structure and their correlating planars exist as shown by XRD results in Figure 2.9b-c. A few characterization methods are also essential to understand a few aspects of the studies, such as the formation mechanism, growth direction, the elements involved to fabricate, and enhance the properties of such materials (e.g: photoluminescence properties in Figure 2.9d) in its respective application.

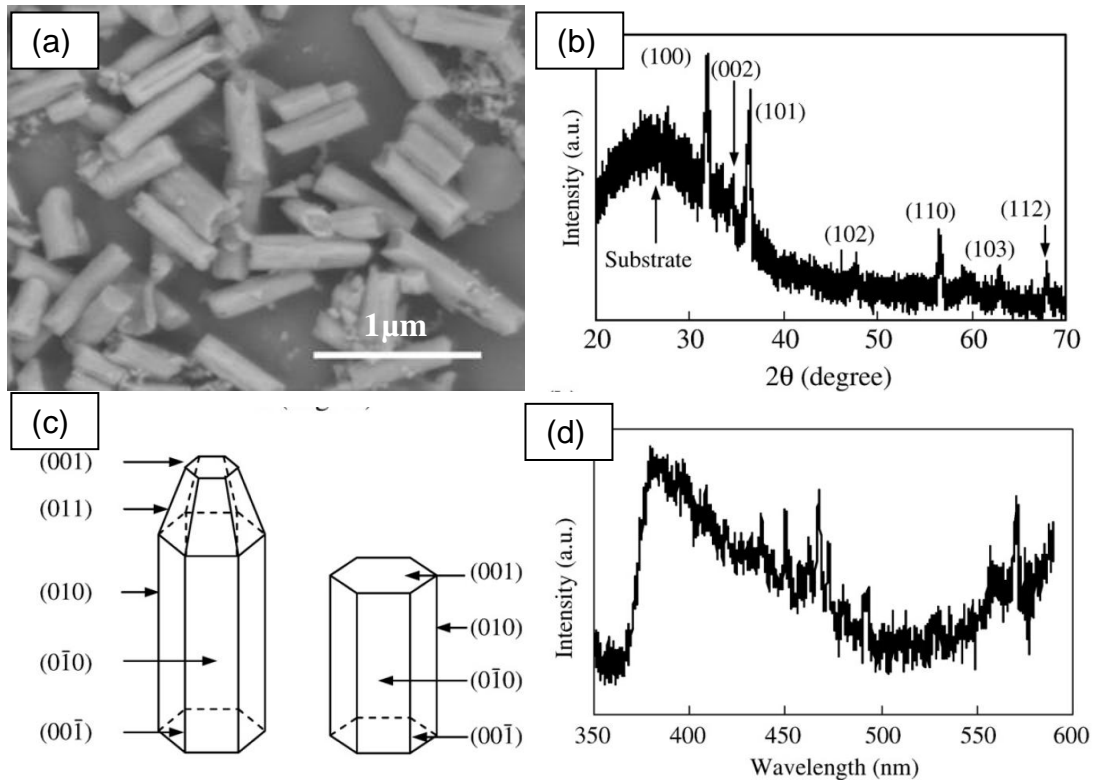


Figure 2.9: A compilation of (a) SEM image; (b) XRD identification; (c) growth structure; and (d) photoluminescence property of fabricated ZnO nanorods (Lee *et al.*, 2008).

2.1.5 Formation Mechanism of Zinc Oxide

The ZnO with different forms of controlled nanostructures are widely studied in recent years. Many types of interesting and delicate ZnO nanostructures have been fabricated so far, which thereby leads to a challenge on the formation mechanism proposal. Generally, the formation of wurtzite structure ZnO crystal is described schematically as two alternating planes composed of four coordinated oxygen ion $[O^{2-}]$ and zinc ion $[Zn^{2+}]$ ions along the c-axis (Figure 2.7).

The proposal by Zhou *et al.* (2008) of ZnO formation in aqueous solution may result in the anisotropic growth of ZnO crystals along the [0001] direction for its growth units ($\text{Zn}(\text{OH})_4^{2-}$) tend to adhere to the (0001) plane. This adherence results in fast growth along [0001] direction. Physically observed, ZnO is likely to elongate along the c-axis due to the higher surface energy of the polar (0001) plane (Zhou *et al.*, 2008). This is why many studies observed the hexagonally rod-like ZnO structures (Figure 2.10). Li *et al.* (1999) added that the growth habit of a crystal can reveal its growth mechanism and vice versa. The habit can be determined through the internal structure and external conditions such as potential, temperature, and pH value of the solution (Li *et al.*, 1999) during synthesis.

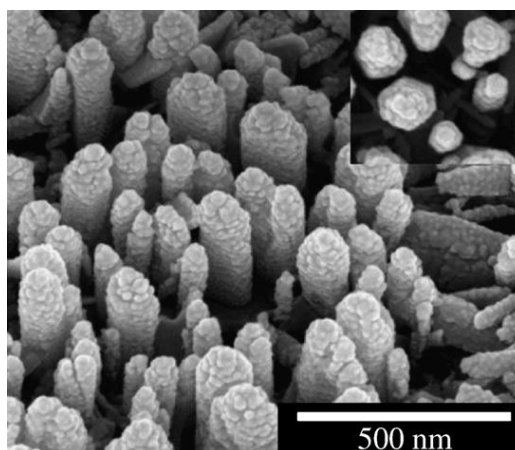


Figure 2.10: SEM image of ZnO nanorods (Breedon *et al.*, 2009).

No works on the effect of synthesis current to the formation via Zn-air system and its formation mechanism were carried out before. The closest example by Xu *et al.*, (2009) showed that by varying the electrodeposition potential significantly affects both preferential growth orientation and growth rate of ZnO nanowires. Figure 2.11a-b shows ZnO fabricated from the aqueous solution containing 0.05 M zinc nitrate [$\text{Zn}(\text{NO}_3)_2$] + 0.05 M hexamethylenetetramine (HMT) at -0.15V, while Figure 2.11c-d was fabricated using 0.05 M $\text{Zn}(\text{NO}_3)_2$ + 0.05 M HMT at -1.1V.

Figure 2.11e schematically shows the formation from flower-like to ZnO nanowire and Figure 2.11f shows the comparison of photoluminescence property between (iii) flower-like and (iv) nanowire.

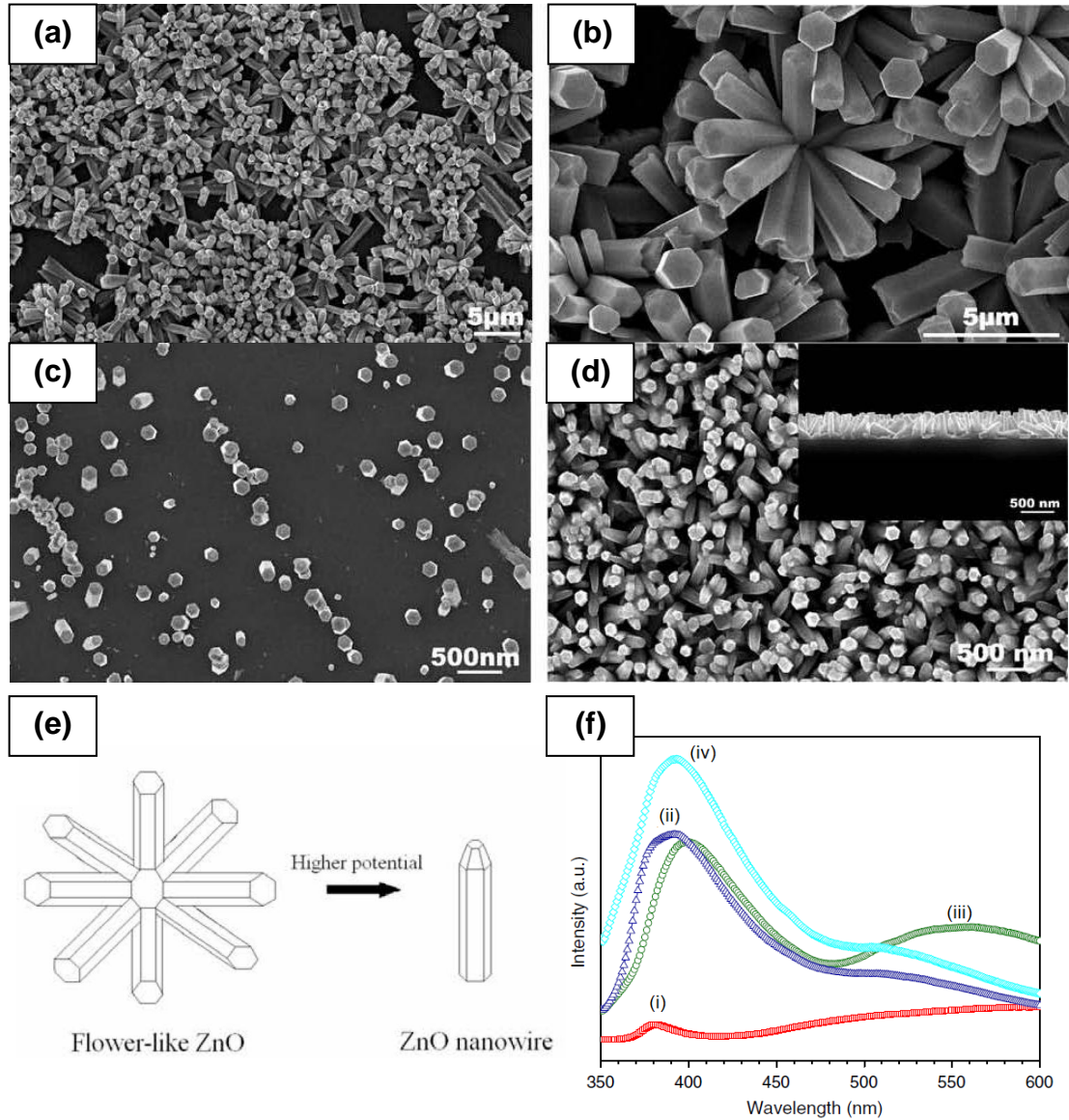


Figure 2.11: An example of a study on the effect of electrodeposition potential in 0.05 M $Zn(NO_3)_2$ aqueous solution (Xu *et al.*, 2009).

Figure 2.11a-d shows the actual morphology evolution from a flower-like ZnO to ZnO nanorods while Figure 2.11e shows the schematic evolution by merely varying the electrodeposition potential. If low electrodeposition potential was applied, the indium tin oxide (ITO) has relatively higher interfacial tension and a few ZnO

crystallites were able to directly absorb and nucleate. Xu *et al.* (2009) suggest that several ZnO crystals pooled a ZnO nucleus for the subsequent growth thus, yielding a flower-like ZnO bundle as shown in Figure 2.11a-b. However, when high electrodeposition potential was applied, the ITO substrate having lower interfacial tension attracts tiny ZnO crystallites to absorb and nucleate thereby resulting in ZnO nanorods (Xu *et al.*, 2009).

A proposal of a formation mechanism does not only enable further interpretation of organization, growth direction, distribution, shapes, and sizes but also the properties of synthesized materials. As an example, Xu *et al.* (2009) describes the photoluminescence property change with respect to its change of morphology fabricated at higher potential. As observed in Figure 2.11f, line (iii) shows a broad green band that lies in the visible region indicating deep level emission due to intrinsic defects, such as zinc vacancy, oxygen vacancy, interstitial zinc or interstitial oxygen itself.

Lines (iii) and (iv) in Figure 2.11f, higher UV emission intensity were observed by line (iv) which may be due to high surface-to-volume ratio of nanorods exposed to excitation: thereby releasing higher emission during detection. This measures the quality of the ZnO by comparing the ratio of relative photoluminescence emission to deep level emission. Due to the fact that the intensity of green band is quite high for flower-like samples, it suggests that the quality of ZnO nanorods produced were better.

Another example on the effect of synthesis temperature is shown in Figure 2.12. Al-Azri *et al.* (2010) recently described the structural change by varying the temperature (a) 1200°C, (b) 1150°C, and (c) 1100°C via carbothermal reduction process to form ZnO (a) wires, (b) tetrapods, and (c) flower-like, respectively. It is observed that the size and morphology change with the effect of temperature. Size enlargement refers back to higher rate of deposition by a reduced starting material caused by external heat energy provided during the ZnO formation. While the morphology on the other hand depends greatly on the catalyst transport, ZnO vapor for the density of vapor varies with temperature. Hence, the morphological difference was affected by the vapor transport and saturation level of the catalyst (Al-Azri *et al.*, 2010).

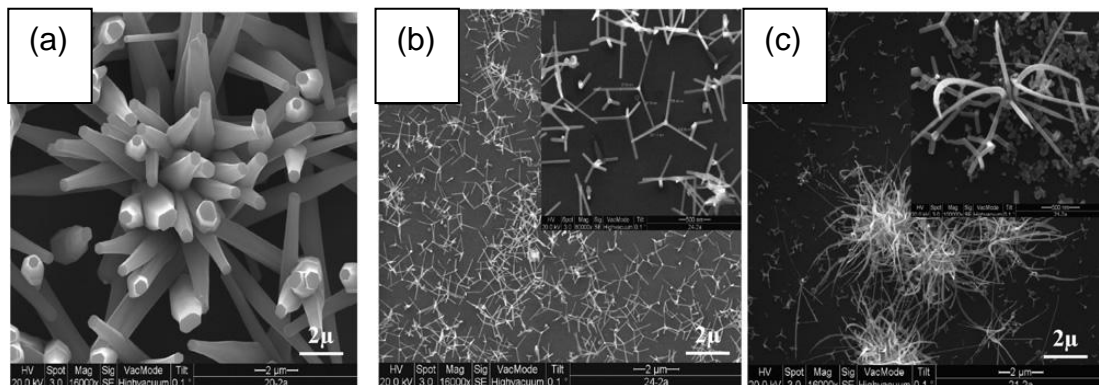


Figure 2.12: Effect of temperature of ZnO grown on Si (100) substrate: (a) 1200°C; (b) 1150°C; and (c) 1100°C (Al-Azri *et al.*, 2010).

Many researchers have proposed the ZnO formation mechanism based on its respective material, preparation, tests, and results. In summary, growth mechanism proposal enables a work to focus on requested property for its application via tuning into favored shapes and sizes of a material and to serve its end purpose.